RESEARCH ARTICLE

Simulating water distribution patterns for fixed spray plate sprinkler using the ballistic theory

Sofiane Ouazaa*, Javier Burguete, M. Pilar Paniagua,
Raquel Salvador and Nery Zapata

Departamento de Suelo y Agua. Estación Experimental Aula Dei (EEAD-CSIC). Apdo. 202. 50080 Zaragoza, Spain

Abstract

Ballistic simulation of the spray sprinkler for self-propelled irrigation machines requires the incorporation of the effect of the jet impact with the deflecting plate. The kinetic energy losses produced by the jet impact with the spray plate were experimentally characterized for different nozzle sizes and two working pressures for fixed spray plate sprinklers (FSPS). A technique of low speed photography was used to determine drop velocity at the point where the jet is broken into droplets. The water distribution pattern of FSPS for different nozzle sizes, working at two pressures and under different wind conditions were characterized in field experiments. The ballistic model was calibrated to simulate water distribution in different technical and meteorological conditions. Field experiments and the ballistic model were used to obtain the model parameters (D_{50}, n, K_1 and K_2). The results show that kinetic energy losses decrease with nozzle diameter increments; from 80% for the smallest nozzle diameter (2 mm) to 45% for nozzle diameters larger than 5.1 mm, and from 80% for the smallest nozzle diameter (2 mm) to 34.7% for nozzle diameters larger than 6.8 mm, at 138 kPa and 69 kPa working pressures, respectively. The results from the model compared well with field observations. The calibrated model has reproduced accurately the water distribution pattern in calm (r = 0.98) and high windy conditions (r = 0.76). A new relationship was found between the corrector parameters (K_1' and K_2') and the wind speed. As a consequence, model simulation will be possible for untested meteorological conditions.

Additional key words: sprinkler irrigation; ballistic model; center-pivot; kinetic energy losses.

Introduction

Impact sprinklers have been replaced by the developments of spray sprinklers commonly used in pivot and linear move irrigation machines. These spray sprinklers use low pressure without affecting to the irrigation quality (Omary & Sumner, 2001). The two main designs of low-pressure spray sprinklers are the fixed spray plate sprinkler (FSPS) and the rotating spray plate sprinklers (RSPS). Comparing FSPS to RSPS, the first are cheaper and robust, while the second present more uniform water distribution pattern (Faci *et al*., 2001; Playán *et al*., 2004). In general, the FSPS has characteristics of large droplets, medium application coverage, minimal wind distortion and low energy requirement. It is important to note that the FSPS with lower price makes it more attractive and competitive than the RSPS.

Abbreviations used: C (aerodynamic drag coefficient); D (drop diameter, mm); D_{50} (mean drop diameter, mm); FSPS (fixed spray plate sprinkler); ID_m (catch can values of measured irrigation depth, mm); $\overline{ID_m}$ (average measured irrigation depths, mm); ID_s (catch can values of simulated irrigation depth, mm); $\overline{ID_s}$ (average simulated irrigation depths, mm); K_1, K_2 (empirical parameters); K_1', K_2' (new empirical parameters); n (dimensionless exponent); P (operating pressure, kPa); P_m (minimum probability for drops smaller than D_{50}); R (coefficient of correlation); RMSE (root mean square error); RSPS (rotating spray plate sprinkler); S_m (standard deviation of measured ID); S_s (standard deviation of simulated ID); U (absolute drop velocity, m s^{-1}); V (relative drop velocity in the air, m s^{-1}); W (wind speed, m s^{-1}); W_d (dominant wind speed, m s^{-1}); α (angle formed by the vectors V and W); β (angle formed by vectors V and U); γ (probability for drops smaller than D); ρ (objective function); Φ (nozzle diameter).

Current center-pivot models are based on the overlapping of experimental sprinkler application pattern (Omary & Sumner, 2001; Delirhasannia *et al*., 2010). Based on semi-empirical considerations and using a combination of beta functions (free from any ballistic consideration), Le Gat & Molle (2000) and Molle & Le Gat (2000) developed a model to simulate the application pattern of a single spray sprinkler, and to describe its performance in both windy and no-wind conditions.

Ballistic simulation (Fukui *et al*., 1980) has been successfully applied to impact sprinklers (Montero *et al*., 2001; Playán *et al*., 2006). Ballistic sprinkler simulation models require information on drop diameter distribution to estimate the landing point and terminal velocity of drops resulting from a certain irrigation event. Procedures have been developed to estimate drop diameter distribution from the sprinkler application pattern using inverse simulation techniques (Montero *et al*., 2001; Playán *et al*., 2006). The percentage of the irrigation water collected at each landing distance can be used to estimate the percentage of the irrigation water emitted in drops of a given diameter. Ballistic theory requires the characterization of the drop diameter distribution. Li *et al*. (1994) proposed an exponential model to characterize the drop diameter distribution for circular and no circular nozzle. Kincaid *et al*. (1996) used this model to fit the drop diameter (D) distribution curve for different type of emitters according to the following equation:

$$\gamma = \frac{0.693 \times n \times (\frac{p}{D50})^n \times e^{\left[-0.693 \times (\frac{D}{D50})^n\right]}}{D} \quad [1]$$

where γ is the probability for drops smaller than D, D_{50} the mean drop diameter, and n is a dimensionless exponent. This empirical model permits to establish a functional relationship between the drop diameter and the sprinkler discharge. The estimation of the parameters of this equation permits to characterize the drop diameter distribution resulting from a given sprinkler, nozzle diameter and operating pressure.

In order to reproduce the deformation of the circular water application area produced by the wind, Seginer *et al*. (1991) and Tarjuelo *et al*. (1994) reported on the need to correct the aerodynamic drag coefficient following this expression:

$$C' = C (1 + K_1 \sin\beta - K_2 \cos\alpha) \quad [2]$$

where C' is the corrected aerodynamic drag coefficient; C is the aerodynamic drag coefficient which can be expressed as a function of the Reynolds number of a spherical drop and the kinematic viscosity of the air (Fukui *et al*., 1980; Seginer *et al*., 1991); β is the angle formed by vectors V (relative drop velocity in the air) and U (absolute drop velocity); α the angle formed by the vectors V and W (wind velocity); and K_1 and K_2 are the empirical parameters determined for each wind velocity conditions. The combination of both parameters has led to significant improvements in the simulation of wind distorted water distribution patterns (Tarjuelo *et al*., 1994). According to Montero *et al*. (2001), K_2 is much less relevant than K_1. Dechmi *et al*. (2004) confirmed this extreme and reported that K_1 and K_2 narrows and displaces, respectively, the water distribution pattern respect to the wind direction.

However, ballistic simulation of the new emitter for self-propelled sprinkler irrigation machines requires the incorporation of the effect of the jet impact with the deflecting plate (Sánchez-Burillo *et al*., 2013). The case of the spray sprinklers commonly used in pivot or linear move irrigation machines differs from impact sprinklers. In this case, the jet produced at the nozzle immediately undergoes an inelastic shock as it frontally hits a plate. Although most spray sprinkler models include certain curvature in the plate and grooves designed to create a number of small jets, the energy lost at the plate is sufficiently large to create uncertainty about the initial velocity of the drops. As a consequence, ballistic models have rarely been applied to the two main designs of spray plate sprinklers.

The shape, ridges and curvature of the deflecting plate determine the number of secondary jets, the vertical initial angle and the drop initial velocity (DeBoer *et al*., 1992). The pressure head at the nozzle, the nozzle diameter and the sprinkler design and manufacturing determine droplet kinetic energy (King & Bjorneberg, 2010). This energy is directly related to drop diameter and velocity (Kincaid, 1996). In kinetic energy analyses of sprinkler irrigation, the drop trajectory and velocity is commonly simulated using an estimation of initial velocity and ballistic simulation models (Kincaid, 1996). Several researchers have characterized the drop kinetic energy in irrigation machines (King *et al*., 2010; King & Bjorneberg, 2012), which are mainly focused on the hydraulic characteristic impact of the soil. Sánchez-Burillo *et al*. (2013) have characterized the drop initial velocity for fixed spray plate sprinkler in order to simulate the effect of the jet impact and incorporate it to the ballistic theory.

In this research the water distribution pattern of FSPSs working at different technical (working pres-

sures) and meteorological conditions (wind speeds) were simulated based on droplet kinetic energy analysis. In this work, the calibration of the ballistic theory to FSPS will be undertaken. Extending the recent efforts in ballistic simulation of impact sprinklers (Carrión *et al*., 2001; Montero *et al*., 2001; Playán *et al*., 2006) to center-pivot spray sprinklers will provide a valuable tool for center-pivot irrigation simulation. This general objective will be performed by the following specific objectives: (1) characterize the kinetic energy losses at the plate of FSPS equipped with different nozzle sizes and working at two different pressures; a technique of low speed photography will be used to determine drop velocity at a certain point just after the plate; (2) characterize experimentally the FSPS water distribution pattern; and (3) calibrate the ballistic model to simulate water distribution patterns of FSPS equipped with different nozzle sizes and working at different technical and meteorological conditions. Field experiments and the ballistic model will be used to obtain the model parameters (D_{50}, n, K_1 and K_2).

Material and methods

The FSPS are usually sprayhead sprinklers that can have different types of interchangeable deflector plates and different interchangeable nozzles (series TN) and thus produce different drop size, throw distance and wind fighting capabilities. The FSPS used in this paper were the D3000 Sprayhead, manufactured by Nelson Irrigation Corporation and corresponded to the series 3TN, with 36-grooved blue plate (#9493) with a medium angle from the horizontal plane (Fig. 1b).

Characterization of velocity and angle of the drops at the exit of the deflecting plate

Ten nozzle diameters at 138 kPa and five nozzle diameters at 69 kPa of the FSPS were selected for experimental characterization of velocities and angles at the exit of the deflecting plate. The selected nozzle diameters (ranging from 2.0 mm to 8.7 mm) and working pressures represent the operational possibilities of a commercial pivot equipped with FSPS. The photographical method proposed by Salvador *et al*. (2009) was used. This technique is based on low speed photography (1/100 s) of the sprinkler droplets as they travel from the sprinkler to the soil surface. The method requires intense illumination, which may be easily obtained in the local conditions by outdoor operation near solar midday. In these circumstances the drops are
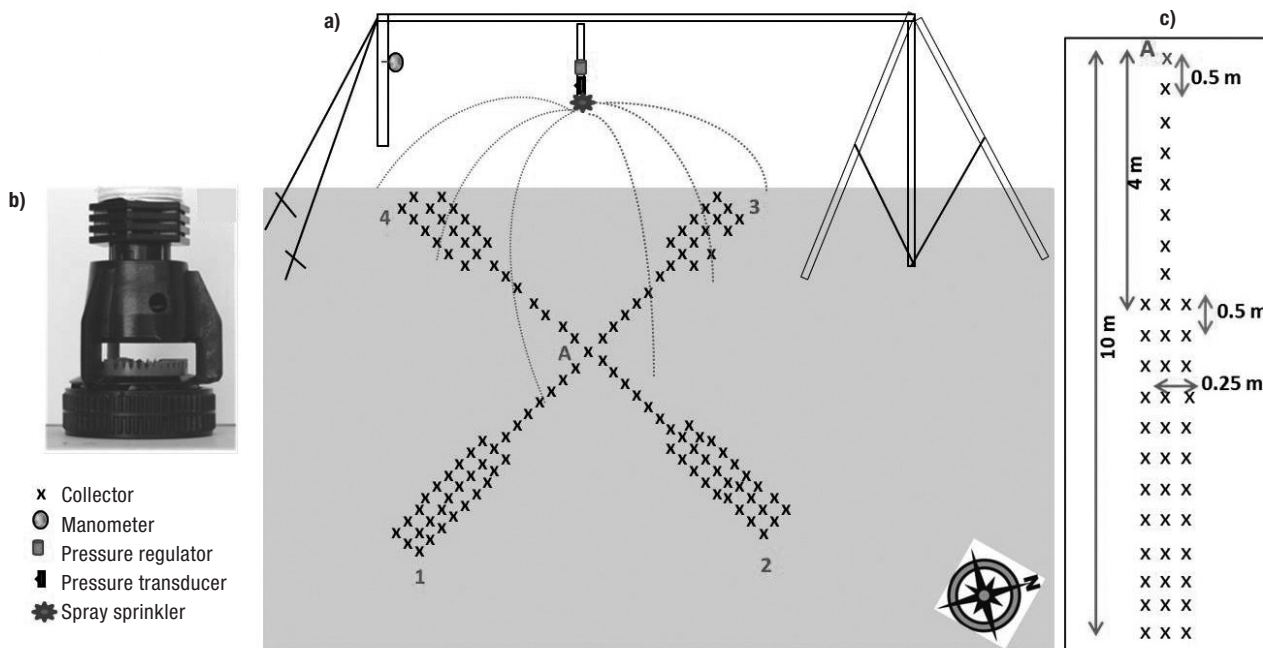

Figure 1. Layout of the collector rows and the spray sprinkler experiment: (a) the set-up of the spray sprinkler over the center of the collector array; (b) the fixed spray plate sprinkler (FSPS) model evaluated; and (c) the layout of the collector array.

photographed as cylinders whose diameter corresponds to the drop diameter and whose length is equivalent to the drop displacement during 1/100 s. This technique permits the determination of cross-sectional diameter, tangential velocity and vertical angle of individual drops located at different distances from the emitter (Salvador *et al*., 2009). Drop photographs were taken at an average horizontal distance of 0.75 m from the FSPS. Sánchez-Burillo *et al*. (2013) reported that FSPS jets visually break into individual drops at a distance of 0.7-0.8 m from the FSPS. Measured drop velocities result from subtracting (from the main jet energy) the head losses due to impact on the deflecting plate and the jet energy losses between the deflecting plate and the measurement point. Simulation techniques based on the inverse solution of drop trajectory (Sánchez-Burillo *et al*., 2013) were applied to estimate droplet head losses between the deflecting plate and the measurement point. A minimum of 40 drops per nozzle size were selected for measurements. The selection of the drops was performed based on image quality since the drop should be adequately focused (located near the vertical plane containing the reference ruler). Drops not reaching 0.3 mm in diameter were discarded since it was impossible to assess if they were focused. The average and standard deviation of the 40 drops initial velocities were obtained for each nozzle diameter. A relationship between nozzle diameter and drop velocity was established to infer drop velocity for unmeasured FSPS nozzle diameters.

The aim of this part of study is to estimate the velocity of the drops after the impact of the jet on the sprinkler deflecting plate. Main differences between the velocities measured at the nozzle and the estimated drop velocities after the impact were attributed to the energy losses at the plate.

Experimental characterization of FSPS water distribution pattern under different technical and meteorological conditions

In this part of study, six different nozzle diameters were selected (2.4 mm, 3.8 mm, 5.1 mm, 6.7 mm, 7.9 mm and 8.7 mm). Nozzles tests were carried out at two working pressures of 103 kPa and 138 kPa (habitual operating pressures for FSPS), maintained by pressure regulator installed just upstream the spray sprinkler. Furthermore, for each combination of nozzle size and working pressure field tests were carried out at 3 different wind velocity levels, calm (W ≤ 1 m s^{-1}), medium (1 ms^{-1}< W ≤ 3 ms^{-1}) and high (W > 3 m s^{-1}). The evaluation of the water distribution pattern for each nozzle diameter, operating pressure and wind velocity was performed individually. An isolated sprinkler nozzle was mounted on a metal frame in the center of a collector array (Fig. 1a). Sprinkler nozzle was located 2.0 m above the soil surface using a semi-rigid plastic drop pipe. Faci *et al*. (2001) reported on the difficulty to characterize FSPS water distribution patterns by catch-can experiments. Most of the applied water for the FSPS is in a circular crown with a width of about 1 m. Water application within the crown was not uniform. Alternate radii with very different depths of water applied could be observed, corresponding to the grooves of the deflector plates. The volume of water applied outside the crown was negligible (Faci *et al*., 2001). A special catch can arrangement was required to capture this peculiar water application pattern. Catch cans were distributed along four principal radii at a distance from the sprinkler ranging from 0.5 m to 10 m, with an increment of 0.5 m. The chosen catch can spacing, 0.5 m, was lower than the crown width, representing a compromise between accuracy and manageability. A finer square network would require a very large number of catch cans, rendering the experiment very time demanding. Each radius had two reinforcement collector lines at the crown area (Fig. 1c). Catch cans were conical in its lower part (200 mm height) and cylindrical in its upper part (100 mm height); the diameter of the upper part was 160 mm. The catch cans were marked in millimetres for direct readout up to 45 mm. An automated weather station located in the experimental field recorded air temperature, relative humidity, and wind speed and wind direction at 1 second intervals. The operating pressure was monitored every 2 minutes by a pressure transducer (Dickson, PR150) installed just downstream the regulator and upstream the FSPS (Fig. 1a). The experimental tests were performed in bare soil and the duration of each test depended on nozzle diameter (from 40 min to 120 min).

Model calibration

The ballistic model was used in this study to simulate the landing distance of different drop diameters resulting from the FSPS for a different nozzle diameter, nozzle elevation and operating pressure. Ballistic

theory considers the wind effect as the main factor of the drops trajectory distortions (Fukui *et al.*, 1980; Playán *et al.*, 2006). Accordingly, a sprinkler is simulated as a device emitting drops of different diameters. It is assumed that drops are formed at the sprinkler nozzle, and travel independently until reaching the soil surface (or the crop canopy, or the experimental catch-can).

The movement of each drop was solved in the model using a second order Runge-Kutta numerical integration technique (Suppl. Table S1 [pdf online]). The main result of each drop trajectory solution is constituted by the x and y coordinates of the drop when the z coordinate is equal to zero (soil surface). In order to reproduce the water application pattern of the isolated FSPS, the model used 320000 drops corresponding to 1600 horizontal sprinkler angles and 200 drop diameters, evenly distributed between 0.0002 m and 0.007 m. The model also used as input data: the drop velocity and the vertical angle of individual drops located after the jet impact (characterized by the above mentioned photographic method), the drop diameter distribution (D_{50} and n) and the drag coefficient parameters (K_1 and K_2). The model of drop diameter distribution used in this work was the exponential type proposed by Li *et al.* (1994) (Eq. [1]). The parameters of the drop diameter distribution model were obtained from the field catch can experiments for six nozzle diameters. Relationships between nozzle diameter and parameters D_{50} and n were established using regression analyses. The objective was to explore possibility of interpolating parameters to simulate unmeasured nozzle diameters in the experimental range. To obtain the best combination of D_{50} and n model parameters, two indexes are used for the comparison between measured and simulated water application: the Root Mean Square Error (RMSE, Eq. [3]) and the coefficient of correlation (r, Eq. [4]):

$$RMSE = \sqrt{\frac{\sum_{i=1}^{N}(ID_m - ID_s)^2}{N}} \qquad [3]$$

$$r = \frac{\sum(ID_m - \overline{ID_m})(ID_s - \overline{ID_s})}{(N-1)\,S_m\,S_s} \qquad [4]$$

where N is the number of catch cans; ID_m and ID_s are the catch can values of measured and simulated irrigation depth; $\overline{ID_m}$ and $\overline{ID_s}$ are the average measured and simulated irrigation depths; and S_m and S_s are the standard deviation of measured and simulated ID. The

coefficient ρ (Eq. [5]) was used as the objective function for the optimization algorithm. The optimum value of ρ is the best combination of low values of RMSE with high values of *r*.

$$\rho = \frac{RMSE}{1 + r} \qquad [5]$$

The calibration of the parameters K_1 and K_2 was performed once D_{50} and n model parameters were calibrated. A second phase of model calibration is required at this point, since adequate values for K_1 and K_2 must be identified. The calibration and validation of K_1 and K_2 were performed in two steps. Field experiments carried out in windy conditions were used. The wind speed (W) and wind direction were determined for each irrigation events in order to incorporate it to the model. The first step optimize K_1 and K_2 values by comparison between measured and simulated irrigation depths, the above-mentioned indexes (RMSE, *r* and ρ) were used for optimization purposes. A second step of the calibration process was performed to obtain K_1 and K_2 as a function of wind speed and nozzle size.

For the calibration processes, the Monte-Carlo simulation methods (Fishman, 1995) were used. This method is a brutal force algorithm that calculates the values of the calibration parameters with pseudo-random numbers. Although the method has a slow convergence, is very robust and it does not remain in local minimum values.

Results and discussion

Kinetic energy losses in the FSPS

The inverse solution applied to estimate jet kinetic energy losses for the drop trajectory from the plate exit point to the drop velocity measurement point (average 0.7 m) showed average values of 1%. This value was deemed negligible in comparison with the values of the photographic method, and was not considered in this study.

Measured drops velocities for the evaluated nozzle diameters and operating pressures are presented in Fig. 2a. Measured drop velocities after the deflecting plate result much smaller than the velocity estimated at the nozzle. This difference is due to the jet impact with the deflecting plate that causes a kinetic energy loss. The results indicate that drop velocity after the deflecting plate changes with the nozzle size, increa-
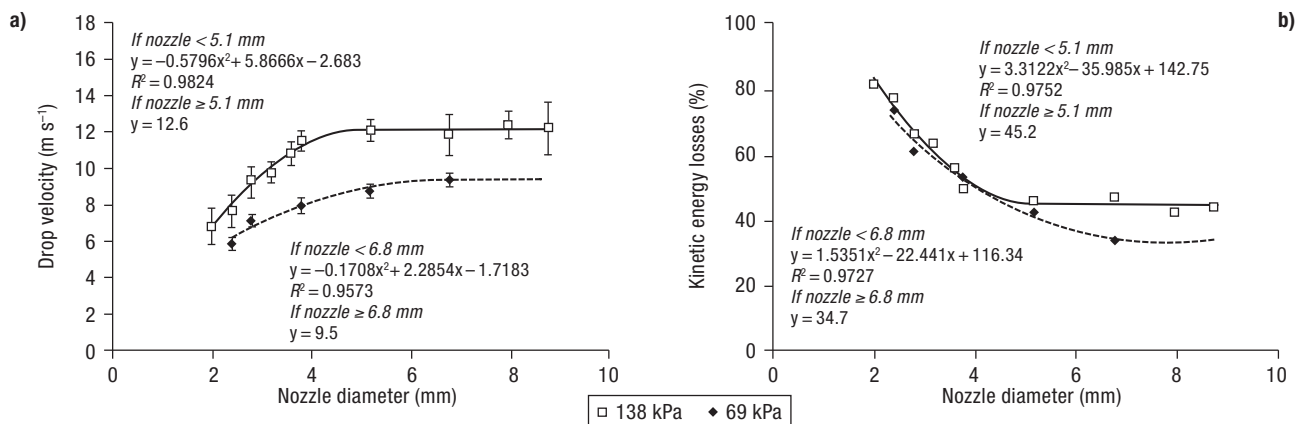
Figure 2. Measured drop velocity (a) and estimated kinetic energy losses (b) as a function of nozzle diameter and at two operating pressures. Vertical bars represent ± the standard deviation of the average for the 40 measured drops.

sing as the nozzle size increases. A regression model was developed to estimate drop velocity for non-measured nozzle diameters. For the largest evaluated pressure (138 kPa) the model was divided in two parts; with the first that (applying to nozzle diameter ≤ 5.1 mm) is following a polynomial model (Fig. 2a) and the second part (applying to nozzle diameter > 5.1 mm) showing a constant velocity value (12.6 m s^{-1}). Moreover, for the smallest evaluated pressure (69 kPa) the model was similar and was also divided in two parts. The first (applying to nozzle diameter ≤ 6.8 mm) follows a polynomial model, and the second (applying to nozzle diameter > 6.8 mm) shows a constant velocity value (9.5 m s^{-1}).

The velocity of the primary jet just outside the nozzle was independent of the nozzle diameter, since nozzles were equipped with a pressure regulator. The impact with the deflecting plate produced large kinetic energy losses whose magnitude depends on nozzle diameter to a maximum diameter value. As the nozzle diameter and jet size increase, impact kinetic energy losses decrease and eventually reach a stable minimum value (Fig. 2b). The shape of the jet impact area on the grooved plate changes with the jet thickness, explaining the experimental differences on kinetic energy losses. For the nozzle diameters < 5.1 mm and for the two evaluated pressures, the kinetic energy losses are similar and reached about 80% of total for the smallest nozzle size (2 mm). For the largest measured nozzles, larger than 5.1 mm at 138 kPa and larger than 6.8 mm at 69 kPa, the kinetic energy losses remained constant around 45% and 34.7% of total, respectively. The kinetic energy losses as a function of nozzle diameters have been incorporated in the ballistic model to simu-

late the FSPS water distribution pattern. A regression model was developed to estimate kinetic energy losses for non-measured nozzle diameters (Fig. 2b). A lineal interpolation (between the values of 138 kPa and 69 kPa) were performed for every nozzle diameter, to estimate kinetic energy losses for non-measured operating pressure of 103 kPa.

For the evaluated FSPS, the vertical angle of individual drops located after the jet impact was independent of the nozzle diameter and the operating pressure. This vertical angle remained constant and is equal to 10 degrees.

Kincaid (1996) proposed a prediction model for the energy loss in FSPS based in the ratio between nozzle and plate diameters. Kincaid's model does not take into account elements that can strongly affect the energy loss, such as plate shape or deflection angle. Sánchez-Burillo *et al*. (2013) characterized the initial drop velocity in FSPS (equipped with one, two and three plates) only at one operating pressure and for three different nozzle diameters. They found that the losses in kinetic energy amounted to 33-55%.

Calibration of the ballistic model

Experimentally measured radial water application patterns are presented in Fig. 3 for the six nozzle diameters at two operating pressures. The water distribution pattern was different for each nozzle diameter and operating pressure. A progressive increasing of the maximum application rate occurs with nozzle diameter, mainly to 5.2 mm and 6.7 mm nozzle size. Moreover, the maximum application rate displaced from the emitter with the
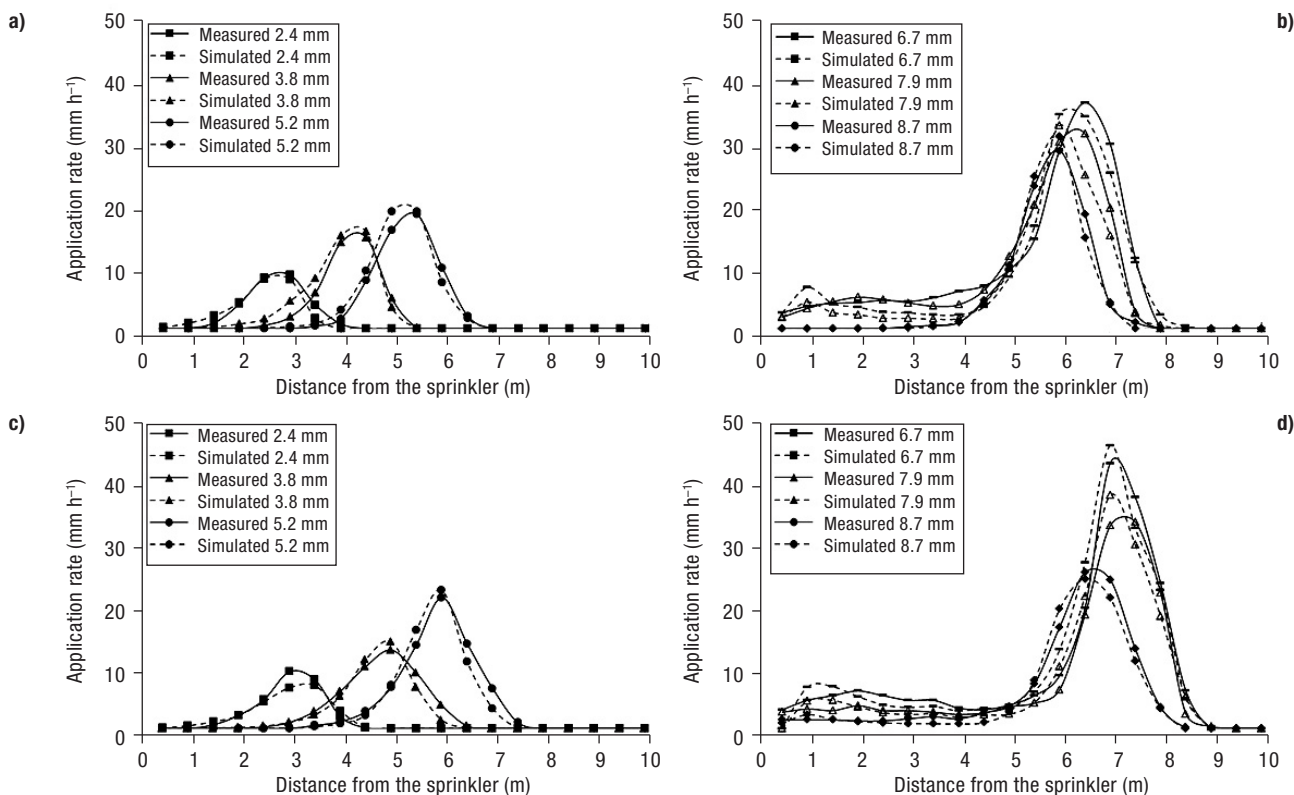
Figure 3. Measured (solid lines) and simulated (dashed lines) radial water application pattern for the experimental FSPS operating at 103 kPa (a and b); and at 138 kPa (c and d).

nozzle diameter and operating pressure increments.

The water application patterns of the three largest nozzles and for the two evaluated pressures (Figs. 3b and 3d) were not symmetrical, with the left tail being longer and higher than the right tail. This behaviour could not be explained by the drop size distribution function used in the ballistic model (Eq. [1]). A modification of the drop size distribution model was introduced to ensure a more realistic simulation. For drop diameters equal to or larger than the mean drop diameter (D_{50}), the probability function was computed using Eq. [1], while for drop diameter lower than D_{50}, the probability was computed as following:

$$\gamma' = \begin{cases} Max\ (\gamma;\ P_m \times \gamma_{D50}),\ D < D_{50} \\ \gamma,\ D \geq D_{50} \end{cases} \qquad [6]$$

where P_m is a new parameter and represents the minimum probability for drops smaller than D_{50}.

The model was run for 396 combinations of D_{50}, n and P_m, with D_{50} values from 1 to 3 mm, n values from 1 to 10, and P_m values from 0 to 1. The main results of the calibration parameters, D_{50}, n and P_m, for the different nozzle diameters and working pressures are pre-

sented in Table 1. The correlation coefficients (*r*) between measured and simulated water distribution was very high, with values larger than 0.97 for the entire range of measured nozzle diameters and operating pressures. Differences between measured and simulated radial water application patterns were very low, with RMSEs ranging from 0.62 mm h⁻ for the smallest nozzle diameter (2.4 mm) to 2.76 mm h⁻¹ for the largest nozzle diameter (8.7 mm), and from 0.66 mm h⁻¹ for the smallest nozzle diameter (2.4 m) to 2.52 mm h⁻¹ for the largest nozzle diameter (8.7 mm), at 103 kPa and 138 kPa operating pressures, respectively. Part of the errors could be attributed to experimental field conditions where the wind velocity is never zero. The water distribution patterns of the six nozzle diameters characterized in this study were simulated with the calibrated parameters. Fig. 3 presents the measured and simulated water application patterns. A very good agreement between simulated and measured water distribution patterns for the three smallest nozzle diameters were observed for both working pressures. A small difference could be observed for the largest nozzle size overall working at 103 kPa (Fig. 3b). Errors could

Table 1. Selection of model parameters D_{50} and n for each nozzle diameter and working pressure

Pressure	Nozzle diameter (mm)	Discharge (m³ h⁻¹)	D_{50} (mm)	n (–)	P_m (–)	RMSE (mm h⁻¹)	r
103 kPa	2.4	0.23	1.1	4.5	0.0	0.62	0.97
	3.8	0.58	1.3	5.7	0.0	0.94	0.98
	5.2	1.10	2.0	7.3	0.0	0.99	0.99
	6.7	1.82	2.3	7.5	0.0	1.08	0.99
	7.9	2.53	2.4	6.5	0.3	2.75	0.97
	8.7	3.07	2.5	6.0	0.4	2.76	0.97
138 kPa	2.4	0.27	1.2	4.6	0.0	0.66	0.98
	3.8	0.68	1.6	6.4	0.0	0.87	0.98
	5.2	1.27	2.0	8.0	0.0	1.17	0.98
	6.7	2.11	2.4	8.0	0.2	1.21	0.99
	7.9	2.93	2.5	7.4	0.4	2.17	0.98
	8.7	3.55	2.5	7.0	0.5	2.52	0.98

RMSE: root mean square error. *r:* coefficient of correlation.

be attributed to field conditions as described before. However, the calibrated model reproduced adequately the water distribution pattern for the different nozzle sizes and operating pressures in the absence of the wind.

Calibrated values of P_m for the experimentally characterized nozzle diameter at two working pressures (symbols) are shown in Fig. 4c. A regression model was developed to interpolate the value of P_m for non-measured nozzle diameters. The model was divided in two parts, the first part that is a constant equal to cero ($P_m = 0$) operates for nozzle diameters smaller than or equal to 5.1 mm for the 103 kPa working pressure, and 6.6 mm for 138 kPa working pressure. The second part, represented by lineal model (Fig. 4c), operates for nozzle diameters larger than 5.1 mm and 6.6 mm, for 103 kPa and 138 kPa working pressures, respectively.

Calibrated parameters D_{50} and n are shown in Figs. 4a and. 4b, respectively. Regression models were developed to interpolate the parameters for unmeasured nozzle diameters within the measurement range. The parameter D_{50} increases with nozzle diameter from 1.1 mm (2.4 mm nozzle diameter) to 2.5 mm (8.7 mm nozzle diameter) for 103 kPa, and from 1.2 mm (2.4 mm nozzle diameter) to 2.5 mm (7.9 mm and 8.7 mm nozzles diameters) for 138 kPa operating pressure. The differences in mean drop diameter between the two evaluated working pressures were small. The value of n increases with nozzle diameter till a nozzle diameter of 6.7 mm, and decreases for larger nozzle diameters. The values of D_{50} and n are slightly affected by the operating pressure for the evaluated range, being

the results of 103 kPa slightly lower than those of 138 kPa. The calibrated values for the n parameter resulted very large indicating an important uniformity of drop sizes, which is reasonable since most of the applied water for the FSPS landed in a circular crown with a width of about 1 m. Similar results of D_{50} values were reported by Kincaid *et al.* (1996) using different methodologies for the same type of sprinklers. Moreover, a similar behavior of the parameter n with nozzle diameters was reported by Playán *et al.* (2006) working with impact sprinklers.

The results of the calibration process for the correction parameters of the aerodynamic drag coefficient, K_1 and K_2 (Eq. [2]), are presented in Table 2. Meteorological conditions of the evaluated irrigation events (wind speed and direction), statistics values used of the optimization process and K_1 and K_2 values are reported in Table 2. The correlation coefficients ranged from 0.56 to 0.91, for the 103 kPa operating pressure and from 0.50 to 0.94 for the 138 kPa, with an average value for both pressures of 0.76. The highest values of the correlation coefficients were obtained for the simulation of water distribution patterns under windy conditions. The RMSE ranged from 1.13 to 11.21 mm h⁻¹, with an average of 5.15 mm h⁻¹, for 103 kPa and from 1.03 to 12.47 mm h⁻¹, with an average of 5.42 mm h⁻¹, for 138 kPa. Highest RMSE values (around 10 mm h⁻¹) were obtained for the largest nozzle diameters (7.9 mm and 8.7 mm) for both working pressures. The statistical parameters showed the capacity of the model to simulate and reproduce the water distribution pattern in medium and high windy conditions.
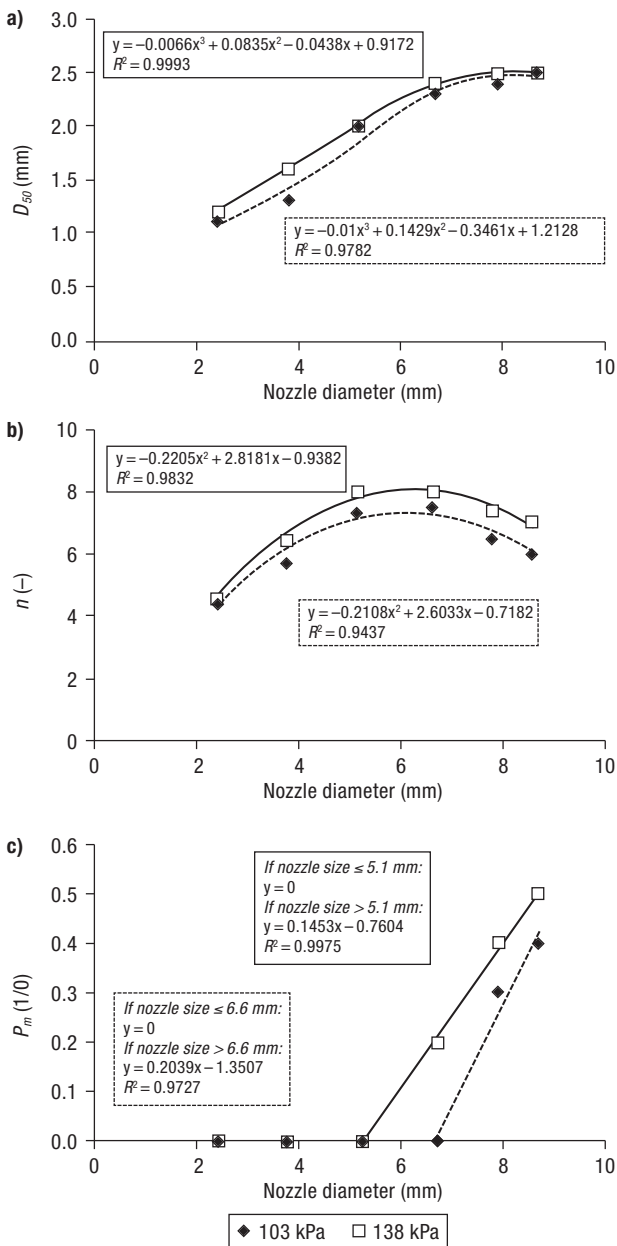
Figure 4. Ballistic model parameters for the experimental FSPS operating at 138 kPa (continuous line) and 103 kPa (dashed line): (a) parameter D_{50}; (b) parameter n and (c) parameter P_m as a function of nozzle diameter.

Figs. 5a and 5b present the relationships between wind speed and the correction parameters of the aerodynamic drag coefficient, K_1 and K_2, respectively. No correlations were found between wind speed and the magnitude of the two correction parameters at the two different operating pressures. K_1 values ranged from 0.0 to 3.6, while K_2 ranged from 0.0 to 1.0, for the evaluated wind conditions. In high windy condi-

tions (> 3.8 m s^{-1}), the exponent K_2 values are equal to zero, otherwise the wind effect is higher on the correction parameter K_1 than K_2.

Although the results may seem contradictory, it has to be noted that the experience in K_1 and K_2 estimation is based on impact sprinklers, in which the jet is very compact. However, our visual experience with FSPS was that the small jets disintegrated completely out the plate under strong wind conditions. Since K_1 and K_2 parameters reflect jet dynamics, it is not illogical that under strong wind conditions the pure ballistic model (with zero K_1 and K_2) well reproduces drops trajectories of FSPS.

The previous process provides values of K_1 and K_2 parameters for evaluated wind conditions. A further research effort was needed to extend the extrapolation of the parameters to other non-evaluated windy conditions. Several probability distribution functions were evaluated to fit the variability of K_1 and K_2 parameter as a function of wind speed and nozzle diameter. The Rayleigh distribution function (Siddiqui, 1961) was finally selected due to its flexibility and because is the best-fitting to the data. The Rayleigh model (Eq. [7]) follows the variability observed in Figs. 5a and 5b and introduces as independent variables nozzle diameter and wind velocity.

$$K_i' = a \times (1 - e^{(-c \times \Phi)}) \times W \times e^{\left[\left(\frac{-b}{1 - e^{(-d \times \Phi)}}\right) \times W^2\right]} \quad [7]$$

where K_i' is the new correction parameter (K_1' or K_2'); Φ is the nozzle diameter; a, b, c and d are empirical parameters; and W is the wind speed.

Table 3 presents the values of the empirical parameters a, b, c and d of the Rayleigh function resulted from the calibration process with the exponential model. Table 4 summarizes the results of the new optimized parameters (K_1' and K_2') and their statistical indexes. The correlation coefficient ranged from 0.16 to 0.91, with an average value of 0.61. The RMSE ranged from 1.17 to 15.65 mm h^{-1}, with an average value of 6.25 mm h^{-1}. According to the values of the statistical indexes, the new models (K_i') performed better than the traditional (K_i) only for the small nozzle diameter (2.4 mm), had similar results for medium nozzle sizes (to 5.2 mm) and performed worse for larger nozzle diameters and overall under strong wind conditions. En general, the efficiency of the model decreased by using the K_1' and K_2' exponential models instead of the traditional K_1 and K_2 models to simulate the wind speed effect on the water distribution patterns.

Table 2. Optimum values of K_1 and K_2 for the different nozzle diameters, wind conditions and operating pressures (103 kPa and 138 kPa). The values of the statistical parameters are also presented

Nozzle size (mm)	W_d (m s⁻¹)	Wind direction	103 kPa				138 kPa			
			RMSE (mm h⁻¹)	r	K_1	K_2	RMSE, (mm h⁻¹)	r	K_1	K_2
2.4	0.8	SSE					1.22	0.75	0.1	0.0
	1.82	NW	1.43	0.66	0.0	1.0				
	2.16	S					1.59	0.66	0.0	0.2
	6.34	NW					1.62	0.62	0.6	0.0
	7.87	NW	1.13	0.83	0.3	0.0				
3.8	0.87	N	2.48	0.75	0.0	0.1				
	1.19	NW					1.44	0.89	1.2	0.2
	2.11	N					1.03	0.90	1.2	0.0
	4.37	NW	2.13	0.87	0.4	0.0				
	6.06	WNW	1.65	0.91	0.2	0.0				
	6.97	WNW					1.67	0.93	0.6	0.0
5.2	2.05	SSW					2.83	0.91	0.6	0.0
	2.96	S	2.88	0.89	0.1	0.0				
	4.11	W	3.66	0.73	2.1	0.0				
	5.3	WNW	2.41	0.91	1.2	0.0				
	5.49	WNW					4.56	0.72	1.2	0.0
6.7	1.51	W	5.48	0.70	0.0	0.0				
	1.59	NW					6.03	0.63	0.9	0.3
	2.6	NW					4.86	0.73	3.2	0.0
	5.6	WNW	6.04	0.82	1.2	0.0				
	8.06	WNW					4.41	0.94	0.9	0.0
7.9	0.82	E					9.04	0.65	1.8	0.1
	1.26	S	10.45	0.57	1.4	0.1				
	1.62	SW					7.75	0.76	3.6	0.1
	3.53	WNW	7.92	0.73	2.4	0.7				
	7.57	NW	8.36	0.78	2.1	0.0				
	7.66	WNW					5.63	0.91	1.2	0.0
8.7	0.75	WSW					11.67	0.57	0.8	0.0
	0.91	SW	10.01	0.56	0.1	0.0				
	2.71	SSW					12.47	0.50	0.5	0.2
	5.82	NW					10.06	0.82	2.7	0.0
	6.76	NW	11.21	0.76	2.1	0.0				

RMSE: root mean square error; *r:* coefficient of correlation.

Figs. 5c and 5d present the relationships between wind speed and the new optimized parameters of the aerodynamic drag coefficient, K_1' and K_2', respectively. K_1' values ranged from 0.02 to 0.37, while K_2' ranged from 0.02 to 0.33 for the whole evaluated wind conditions. The K_1' values for the lowest evaluated pressure (103 kPa) were higher than those for the highest evaluated pressure (138 kPa) (slopes in Fig. 5c), while small differences in K_2' values were observed for the two evaluated pressures (slopes in Fig. 5d). For both operating pressures, the wind speed had more influence to narrow the water distri-

bution pattern in the direction perpendicular to the wind, than to displace the wetted area in the wind direction. Fig. 6 presents simulated water distribution patterns for two FSPS nozzle diameters (2.4 mm and 8.7 mm) under two wind conditions (calm wind conditions and windy conditions) and under two working pressures (103 kPa and 138 kPa). The model simulates the nozzle size effect, the pressure and the wind speed as reported the differences between subfigures of Fig. 6.

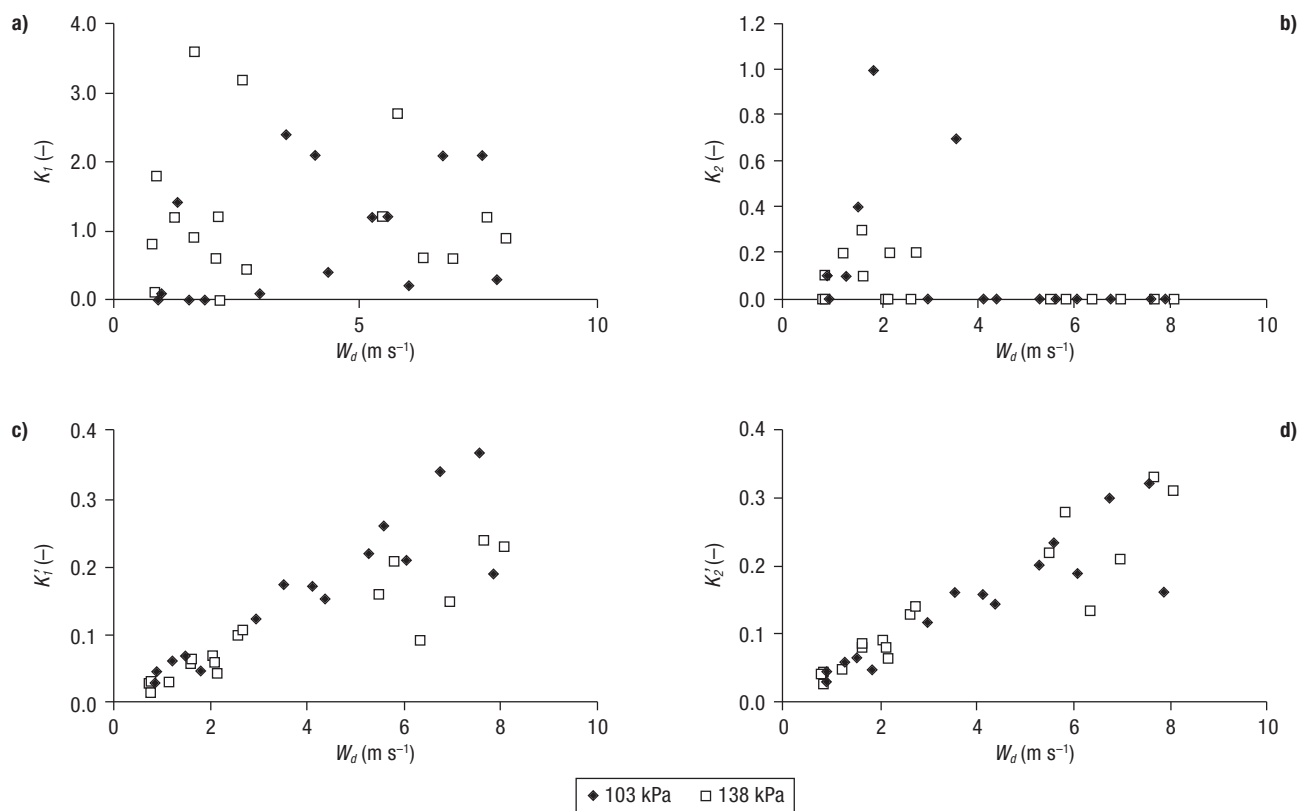This research presents the methodology to simulate FSPS water distribution pattern using droplet kine-

Figure 5. The coefficients K_1 and K_2 (a and b) and the coefficients K_1' and K_2' (c and d) *vs* dominant wind speed, *Wd,* for two working pressures (103 kPa and 138 kPa).

tic energy analysis. The velocity of the drops after the jet impact with the deflecting plate was successfully determined for a combination of nozzle sizes and operational pressures by the photographical method (Salvador *et al*., 2009). The measured drop velocity increases with nozzle size indicating that jet impact head losses decreases as nozzle diameter increases. This relationship may be useful for designing new emitters for center- pivot irrigation systems.

Ballistic models perform reasonably well given an initial drop velocity and size of drop. The ballistic mo-

del parameters were calibrated with field experiment under different technical and meteorological (windy levels) conditions. Experimental results revealed that the FSPS produces a circular crown water distribution pattern which was different for each nozzle diameter and operating pressure.

Good relationships were found between drop diameter distribution curve parameters, D_{50} and *n*, and nozzle diameters for both evaluated working pressures. D_{50} values increases with nozzle diameters and *n* parameter presents a high values always larger than 4. These large values represent a very homogeneous drop size distribution that explains the doughnut-shaped distribution pattern of the FSPS.

The calibrated model has reproduced accurately the water distribution pattern in calm ($r = 0.98$) and high windy conditions ($r = 0.76$). The relationship between the corrector parameters of the aerodynamic drag coefficient (K_1 and K_2) and the wind speed was not clear. Possible reasons of uncertainties in K_1 and K_2 estimations could be that the Monte-Carlo calibration method is bit accurate.

Table 3. Summarized results for calibration parameters for the exponential models for K_1' and K_2'

	103 kPa		138 kPa	
	K_1'	**K_2'**	**K_1'**	**K_2'**
a	0.0580	0.0520	0.0490	0.0600
b	0.0004	0.0011	0.0036	0.0029
c	252.0000	281.8000	241.7000	295.3000
d	265.4000	140.4000	201.7000	164.5000

Table 4. Calibrated values of K_1' and K_2', for the different nozzle diameters, wind conditions and operating pressures (103 kPa and 138 kPa). The table also presents the values of the statistical index obtained in the calibration process

Nozzle size (mm)	W_d (m s^{-1})	Wind direction	103 kPa				138 kPa			
			RMSE (mm h^{-1})	r	K_1'	K_2'	RMSE (mm h^{-1})	r	K_1'	K_2'
2.4	0.8	SSE					1.17	0.77	0.02	0.02
	1.82	NW	1.17	0.77	0.05	0.05				
	2.16	S					1.78	0.59	0.04	0.06
	6.34	NW					1.50	0.67	0.09	0.14
	7.87	NW	1.20	0.84	0.19	0.16				
3.8	0.87	N	2.91	0.67	0.03	0.03				
	1.19	NW					1.72	0.85	0.03	0.05
	2.11	N					1.22	0.84	0.06	0.08
	4.37	NW	2.12	0.88	0.15	0.14				
	6.06	WNW	1.83	0.91	0.21	0.19				
	6.97	WNW					2.00	0.85	0.15	0.21
5.2	2.05	SSW					3.18	0.89	0.07	0.09
	2.96	S	4.51	0.71	0.13	0.12				
	4.11	W	4.21	0.58	0.17	0.16				
	5.3	WNW	3.70	0.76	0.22	0.20				
	5.49	WNW					4.46	0.52	0.16	0.22
6.7	1.51	W	6.90	0.56	0.07	0.07				
	1.59	NW					7.05	0.53	0.06	0.08
	2.6	NW					5.93	0.45	0.10	0.13
	5.6	WNW	8.45	0.51	0.26	0.23				
	8.06	WNW					5.04	0.81	0.23	0.31
7.9	0.82	E					9.58	0.59	0.03	0.04
	1.26	S	10.45	0.56	0.06	0.06				
	1.62	SW					13.06	0.16	0.07	0.09
	3.53	WNW	12.13	0.23	0.18	0.16				
	7.57	NW	10.66	0.46	0.37	0.32				
	7.66	WNW					7.71	0.69	0.24	0.33
8.7	0.75	WSW					12.23	0.52	0.03	0.04
	0.91	SW	9.86	0.55	0.05	0.04				
	2.71	SSW					12.83	0.45	0.11	0.14
	5.82	NW					13.87	0.22	0.21	0.28
	6.76	NW	15.65	0.18	0.34	0.30				

Further research efforts were presented to extend the corrector parameters (K_1 and K_2) for non-evaluated meteorological conditions. An exponential model with wind speed and nozzle diameter as independent variables was proposed to estimate the corrector parameters of the aerodynamic drag coefficient (K_1' and K_2'). This model permits to simulate FSPS water distribution patterns under untested meteorological conditions.

This research will be completed adding to the model the center-pivot dynamic modeling to simulate the whole centre-pivot irrigation.
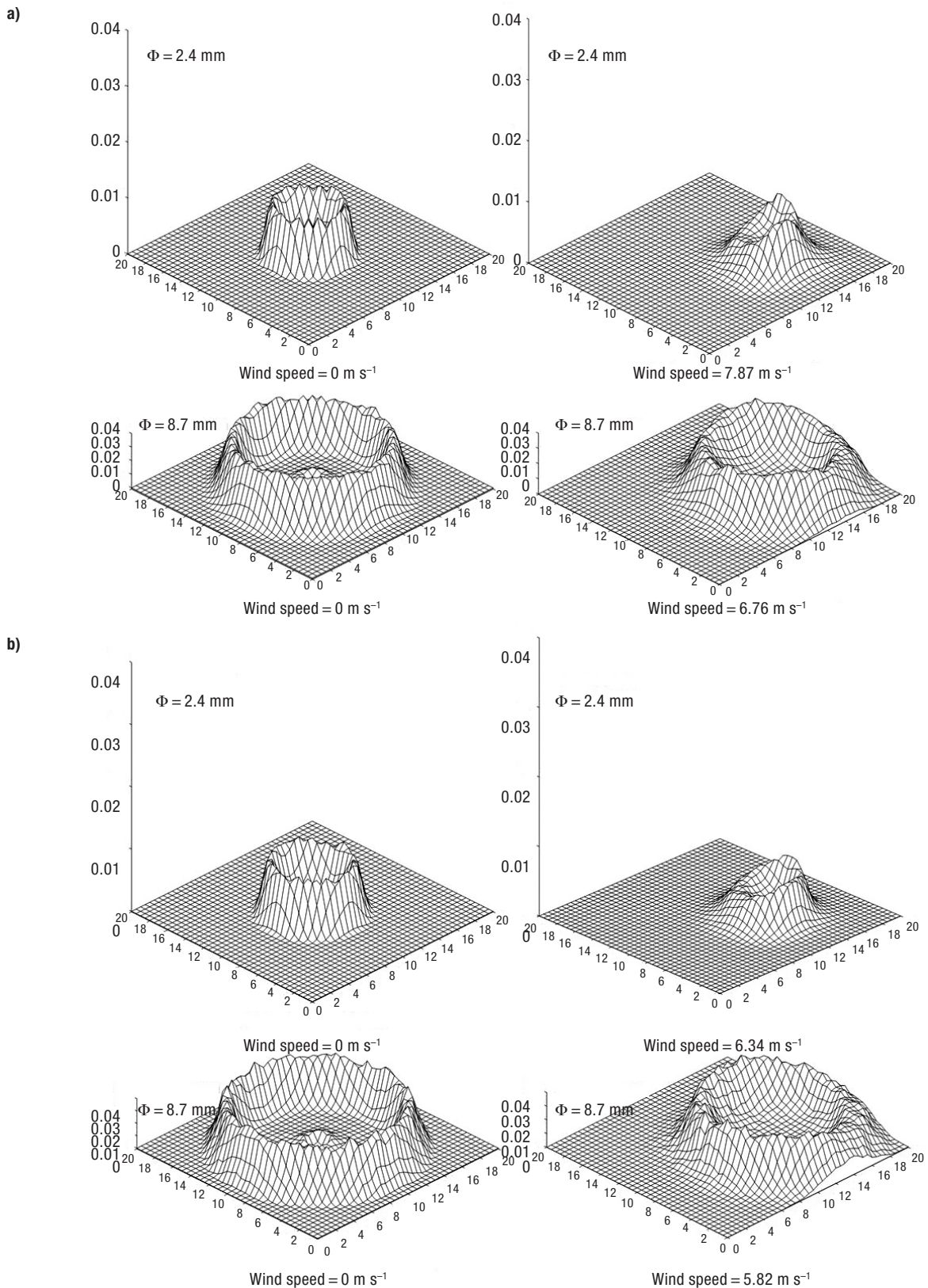
Acknowledgments

Figure 6. Simulated water distribution patterns for two nozzle diameters (2.4 mm and 8.7 mm), two wind speed (calm and strong wind) and two operating pressures (a) 103 kPa and (b) 138 kPa.

gos) for having selected this work to be submitted for publication in this journal.

References

Carrión P, Tarjuelo JM, Montero J, 2001. SIRIAS: a simulation model for sprinkler irrigation: I. Description of the model. Irrigation Sci 20: 73-84.

DeBoer DW, Beck DL, Bender AR, 1992. A field evaluation of low, medium and high pressure sprinklers. T ASAE 35(4): 1185-1189.

Dechmi F, Playan E, Cavero J, Martínez-Cob A, Faci JM, 2004. A coupled crop and solid-set sprinkler simulation model: I. Model development. J Irrig Drain Eng ASCE I130(6): 499-510.

Delirhasannia R, Sadraddini AA, Nazemi AH, Farsadizadeh D, Playán E, 2010. Dynamic model for water application using centre pivot irrigation. Biosyst Eng 105: 476-485.

Faci JM, Salvador R, Playán E, Sourell H, 2001. A comparison of fixed and rotating spray plate sprinklers. J Irrig Drain Eng ASCE 127(4): 224-233.

Fishman GS, 1995. Monte Carlo: concepts, algorithms, and applications. Springer, NY. 621 pp.

Fukui Y, Nakanishi K, Okamura S, 1980. Computer evaluation of sprinkler irrigation uniformity. Irrigation Sci 2: 23-32.

Kincaid DC, 1996. Spraydrop kinetic energy from irrigation sprinklers. T ASAE 39: 847-853.

Kincaid DC, Solomon KH, Oliphant JC, 1996. Drop size distributions for irrigation sprinklers. T ASAE 39(3): 839-845.

King BA, Bjorneberg DL, 2010. Droplet kinetic energy from center-pivot sprinklers. T ASABE, IRR10(8726): 1-11.

King BA, Bjorneberg DL, 2012. Droplet kinetic energy of moving spray-plate center-pivot irrigation sprinklers. T ASABE 55(2): 505-512.

King BA, Winward TW, Bjorneberg DL, 2010. Laser precipitation monitor for measurement of drop size and velocity of moving spray-plate sprinklers. Appl Eng Agric 26(2): 263-271.

Le Gat Y, Molle B, 2000. Model of water application under pivot sprinkler: I. Theoretical grounds. J Irrig Drain Eng 126(6): 343-347.

Li J, Kawano H, Yu K, 1994. Droplet size distributions from different shaped sprinkler nozzles. T ASAE 37(6): 1871-1878.

Molle B, Le Gat Y, 2000. Model of water application under pivot sprinkler: II. Calibration and results. J Irrig Drain Eng 126(6): 348-354.

Montero J, Tarjuelo JM, Carrión P, 2001. SIRIAS: a simulation model for sprinkler irrigation. II Calibration and validation of the model. Irrigation Sci 20: 85-98.

Omary M, Sumner H, 2001. Modeling water distribution for irrigation machine with small spray nozzles. J Irrig Drain Eng 127(3): 156-160.

Playán E, Garrido S, Faci JM, Galán A, 2004. Characterizing pivot sprinklers using an experimental irrigation machine. Agr Water Manage 70: 177-193.

Playán E, Zapata N, Faci JM, Tolosa D, Lacueva JL, Pelegrín J, Salvador R, Sánchez I, Lafita A, 2006. Assessing sprinkler irrigation uniformity using a ballistic simulation model. Agr Water Manage 84: 86-100.

Salvador R, Bautista-Capetillo C, Burguete J, Zapata N, Playán E, 2009. A photographic methodology for drop characterization in agricultural sprinklers. Irrigation Sci 27(4): 307-317.

Sánchez Burillo G, Delirhasannia R, Playán E, Paniagua P, Latorre B, Burguete J, 2013. Initial drop velocity in a fixed spray plate sprinkler. J Irrig Drain Eng 139(7): 521-531.

Seginer I, Kantz D, Nir D, 1991. The distortion by wind of the distribution patterns of single sprinklers. Agric Wat Manag 19: 314-359.

Siddiqui MM, 1961. Some problems connected with rayleigh distributions. The Journal of Research of the National Bureau of Standards, Sec. D: Radio Propagation 66D(2): 169.

Tarjuelo JM, Carrión P, Valiente M, 1994. Simulación de la distribución del riego por aspersión en condiciones de viento. Invest Agr: Prod Prot Veg 9(2): 255-272.